Highly Conductive Zinc Oxide Based Transparent Conductive Oxide Films Prepared Using RF Plasma Sputtering Under Reducing Atmosphere

Ali Salimian [1,*]**, Abul Hasnath** [1]**, Lorna Anguilano** [2]**, Uchechukwu Onwukwe** [2]**, Arjang Aminishahsavarani** [1]**, Cova Sachez** [1] **and Hari Upadhyaya** [1,*]

[1] Centre for Advanced Materials, School of Engineering, London South Bank University, 103 Borough Road, London SE1 0AA, UK; hasnatha@lsbu.ac.uk (A.H.); aminisha@lsbu.ac.uk (A.A.); pardosac@lsbu.ac.uk (C.S.)

[2] Experimental Techniques Centre, Brunel University London, Kingston Lane, Uxbridge UB8 3PH, UK; lorna.anguilano@brunel.ac.uk (L.A.); Uchechukwu.Onwukwe2@brunel.ac.uk (U.O.)

* Correspondence: salimiaa@lsbu.ac.uk (A.S.); upadhyah@lsbu.ac.uk (H.U.)

Abstract: The spectral properties and colour functions of a radio frequency (RF)-based sputtering plasma source was monitored during consecutive sputter deposition of zinc doped indium oxide (IZO) thin films under argon and argon/hydrogen mix. The effect of target exposure to the hydrogen gas on charge density/mobility and spectral transmittance of the deposited films was investigated. We demonstrate that consecutive exposure to the hydrogen gas during the deposition process progressively affects the properties of thin films with a certain degree of continuous improvement in electrical conductivity while demonstrating that reverting to only argon from argon/ hydrogen mix follows a complex pathway, which has not been reported previously in such detail to our knowledge. We then demonstrate that this effect can be used to prepare highly conductive zinc oxide thin films without indium presence and as such eliminating the need for the expensive indium addition. We shall demonstrate that complexity observed in emission spectra can be simply identified by monitoring the colour of the plasma through its colour functions, making this technique a simple real-time monitoring method for the deposition process.

Keywords: sputtering; ZnO; IZO; TCO; plasma; conducting oxides; transparent; hydrogen

---

1. Introduction

Transparent conducting oxide (TCO) thin films are applied in various optoelectronic devices, mobile phone screens, flat panel displays and most importantly in the fabrication of thin film-based solar cell devices, and plasma sputter deposition is one of the main established methods of applying these coatings. The nature of these materials brings about adjustments of dual functionality parameters viz. conductivity and transparency, which requires complex efforts and understanding for the optimization of various sputtering conditions. However, these characteristics are directly related to the complex electronic band configuration of these materials and have been a subject of great attention worldwide [1]. One of the TCO materials that has recently gained interest is zinc doped indium oxide (IZO) due to the robust nature of its resistance against moisture. The parasitic absorption in TCOs as the front window electrode in solar cell configurations such as silicon heterojunctions is a leading factor in undermining cell efficiency. This can be resolved by the application of TCO materials that demonstrate high mobility irrespective of their charge density [1]. Due to the presence of multiple layers in solar cell designs such as CIGS (Copper Indium Gallium di-Selenide) and perovskite devices [2,3], which are sensitive to ambient moisture and temperature, deposition of TCO materials at low temperatures is highly desirable, and hence, IZO stands as a potential TCO material for these applications.

Several techniques exist for the deposition of TCO materials, and plasma sputtering is the most established methodology amongst them [4–6]. The co-sputtering of IZO with hydrogen has been reported to enhance the conductivity of these TCOs with a focus on optoelectronic applications [7,8]. However, we have not noticed a study on the effects of the consecutive coating under hydrogen and the variation it causes to each consecutively prepared sample.

To discuss, develop and engineer the making of these materials it is vital that the mechanism by which these materials demonstrate transparency and conductivity is well-understood and can be repeated during experimental trials. The mechanism by which the bandgap of these materials is specifically altered is referred to as the Moss-Burstein shift, which in simple terms refers to widening the optical bandgap of the material. The Fermi level, work function, ionization energy, energy gap, and electron affinity are fundamental parameters that need to be addressed when discussing TCOs [9]. These parameters define the electronic interface between the TCO surface and other materials and control the charge exchange and transport across these materials. Figure 1 illustrates a simple energy diagram of a semiconductor exhibiting the above-mentioned parameters.
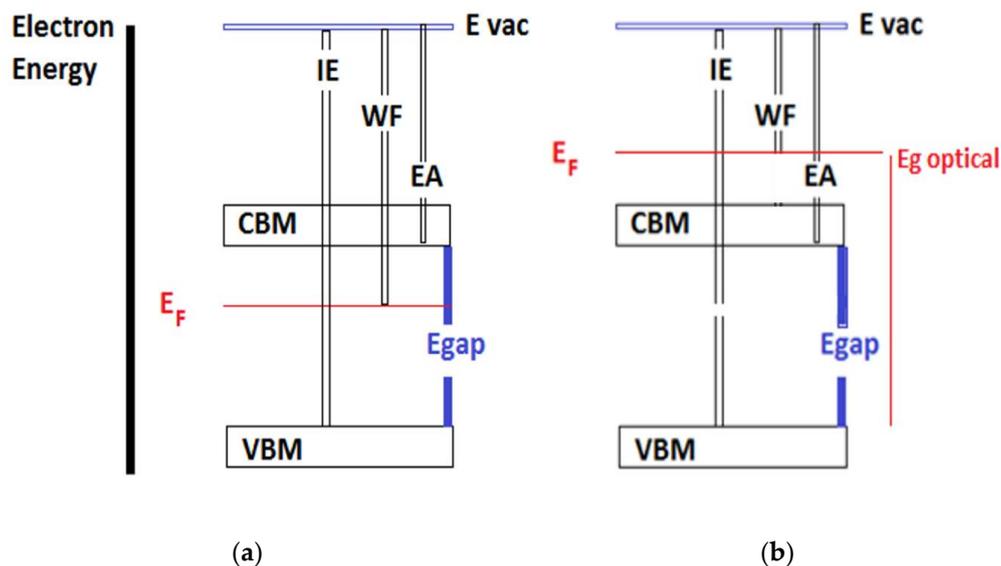

(**a**)   (**b**)

Figure 1. (**a**) A simple flat band representation of the energy band at the surface of a semiconductor (assuming no net charge accumulation at the surface). The ionization energy (IE), work function (WF), electron affinity (EA), fermi level (E_F), bandgap (Eg), optical gap (Eg Optical), conduction band minimum (CBM) and valence band maximum (VBM) are simply defined; (**b**) the schematic diagram showing the optical widening of the transparent conducting oxide (TCO) bandgap using the Moss-Burstein shift, E_g^{MB}.

As electrons are naturally bound to the solid, they are prevented from escaping outside of the material into the vacuum via an energy barrier that culminates at the vacuum level (E_{vac}). Thus, E_{vac} is the energy level of an electron resting within close vicinity outside the solid. At this vicinity, the electron is experiencing the full impact of the surface dipole. To get an electron from the $E_{VB, max}$ into the E_{vac} region, a certain amount of energy is required and this is referred to as the ionization energy (E_I), hence when thinking of n-type doping of a TCO material or a semiconductor, the ideal doping material should have low E_I. If an electron drops from the E_{vac} region into the $E_{CB, min}$ level, it will release some energy, and this is referred to as the electron affinity (E_A) of the material [9]. The work function (Φ) is defined as the energy required to take an electron from the Fermi level and place it in the E_{vac} region. In a semiconductor, the Φ is dependable on the E_{vac}, and the Fermi level (E_F) is governed by the doping concentration, density of states, carrier density and temperature.

In n-type TCOs materials such as indium zinc oxide (IZO), lattice defects in the metal oxide crystal can create an excess of electrons within the vicinity of the defect. Under sufficient orbital

overlap conditions, these electrons can become delocalized and flood the conduction band minimum (CBM). This in a way shifts the Fermi level in a region above the CBM [10]. This effect results in the formation of an optical gap which is now larger than the bandgap of the material and is referred to as the Moss-Burstein shift.

All the parameters discussed so far fundamentally depend on the technique by which the material is produced and prepared. It is ultimately the arrangements of the atoms next to each other that defines the final material's composition and properties. Hence, the preparation technique and operation method of arranging the constituting atoms of a TCO will govern the quality of the produced transparent conductive film.

When sputter deposition of a TCO such as IZO is carried out, one can imagine how vital the sputtering conditions are to the way that the atoms are deposited and laid on the substrate surface, which will ultimately define the work function, electron affinity, band-gap and all the discussed parameters. Most importantly, moving from one sputter deposition unit to another can be challenging in terms of repeatability of the deposition quality against the deposition parameters.

The authors recently reported on implementing a novel approach through which the sputtering plasma can be given a unique fingerprint based on a system identical to the method by which colour functions are utilized in giving an 'x' and 'y' coordinate to a light source to identify its colour [11]. We demonstrated that relationships between the plasma operating parameters such as plasma power and chamber pressure can be established with the colour functions of the plasma. The colour functions are driven from the area under the peaks of the emission spectrum of any light source, and by treating the plasma as a light source we proposed characterizing it based on its colour. In that report, we demonstrated a significant observation regarding the effect of hydrogen on shifting of the colour functions and how these functions behaved once the sputtering target was exposed to hydrogen. In this report, we take a closer look at this methodology with an emphasis on detailed monitoring of the sputtering plasma during IZO preparation with argon (Ar) and argon/hydrogen (5%) gas mix (Ar + H) as the working gas. We shall also demonstrate that consecutive exposure of pure ZnO target to (Ar + H) will improve the electrical properties of ZnO films without any doping.

2. Experimental

The sputtering instrument used for these experiments was a V6000 unit that was manufactured by Scientific Vacuum Systems limited (SVS Ltd., Wokingham, UK) with a vacuum chamber of ~40 cm × 40 cm × 40 cm. The distance between the target surface and substrate (centre to centre) was 15 cm at a 45° angle. The working gases used in the experiment were argon (Ar) and an argon-5%hydrogen (Ar + H) single source; the flow rate of Ar and Ar+H for achieving the desired working pressure in the samples was adjusted accordingly.

IZO samples (S series): The magnetron of the V6000 unit was fitted with a six-inch diameter 99.99% pure indium zinc oxide (IZO) target (In60-Zn40 at %) material with copper indium back bond for efficient thermal dissipation. Using this target, 'seven' IZO thin film depositions were carried out. All the experiments were carried out at ambient temperature for two hours under a 100W RF plasma power and a chamber pressure of 2.3×10^{-3} mbar. During each deposition, four soda-lime glass slide substrates were placed in the chamber and coated with IZO, with the substrate stage rotating at a speed of 20 rpm.

ZnO samples (H series): The magnetron of the V6000 unit was fitted with a six-inch diameter 99.99% pure zinc oxide (ZnO) target material with copper indium back bond for efficient thermal dissipation. Using this target, 'three' ZnO thin film depositions were performed. All the experiments were carried out at ambient temperature for two hours under 150 W RF plasma power and a chamber pressure of 2.3×10^{-3} mbar, as will be described in further detail below. During each deposition, four soda-lime glass slide substrates were placed in the chamber and coated with ZnO, with the substrate stage rotating at a speed of 20 rpm.

All substrates were washed and sonicated with soap water, acetone and ethanol separately to ensure a clean surface before the thin film deposition.

The samples were then tested for film thickness via a profilometer (Veeco, NY, USA); this was carried out by scanning the stylus of the profilometer over a one millimetre strip of deposited films on a soda-lime glass substrate. Optical properties were carried out via UV/VIS spectroscopy (Bibby Scientific Ltd., Staffs, UK). Charge carrier density and mobility were measured using a home-built Hall effect measurements system, with 10 mm × 10 mm substrate sizes and the electrode pads connecting to the four corners of the surface (~1mm into the sample from corner edge).

During each deposition procedure of one of the sample series (which will be discussed in detail), spectral data from the plasma were obtained using an in-vacuum collimator optic probe that was made by Plasus GmbH (Mering, Germany). The probe was installed on the magnetron so that it horizontally collected light from ~1.5 cm away from the surface of the target and at a distance of 4 cm from the edge of the target. The unique feature of the optic collimator is the honeycomb structure of the photon inlet, which traps the sputtering particle and prevents gradual coating of the collimator quartz windows. We have previously demonstrated how this technique will ensure that the collimator lens does not get coated during the sputtering procedure [11]. The collected light was then guided to a Plasus Emicon Spectrometer (Mering, Germany), which generates a detailed spectral plot of the emission. Emicon software (Plasus GmbH, Mering, Germany) coupled to the spectrometer was programmed to calculate the area under the peak of the spectral range based on pre-designated segments of the spectrum. A Jeti Specbos 1201 spectrometer (Jena, Germany) was used to calculate the chromaticity index of the light; the Jeti spectrometer was programmed so that for each measurement, it took 20 readings and inputted the average (Figure 2).
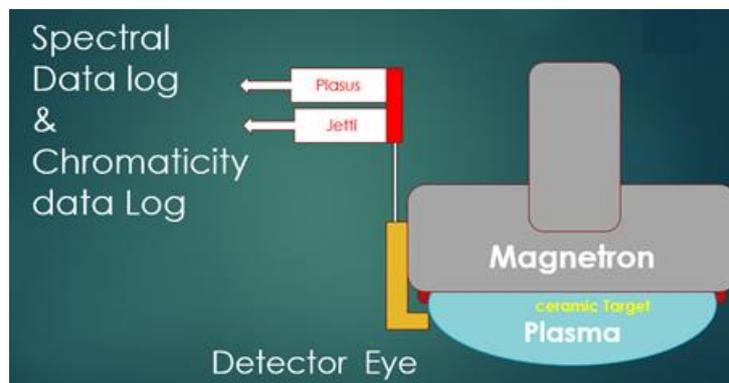

Figure 2. An in-vacuum collimator optic (detector eye) was placed adjacent to the magnetron fitted with a six-inch indium zinc oxide (IZO) target, and the emission data were transferred to the spectrometers via quartz fiber; the distance between the collimator and target edge was 4 cm. The distance between the target surface and substrate (center to center) was 15 cm at 45° angle.

2.1. Indium Zinc Oxide Samples Preparation

During each sample preparation, (using the IZO target), the chamber was placed under vacuum until it reached a base pressure of 1.5×10^{-7} mbar; the seven samples (S1–S7) were prepared using 100 W RF plasma power with a working gas pressure of 2.3×10^{-3} for exactly 2 h under the following protocol.

Samples S1–S4 were prepared using Ar + H (9 sccm) gas, and samples S5–S7 were prepared using Ar only (7 sccm). Sample S5 was hence the point where Ar + H gas mixture was switched to Ar gas only.

S1: During the preparation of this IZO deposition, the target was not exposed to Ar + H gas previously.

S2: As a consecutive to S1 preparation, the target was previously exposed to Ar + H gas for two h.

S3: As a consecutive to S2, the target was previously exposed to Ar + H gas for four h.

S4: As a consecutive to S3, the target was previously exposed to Ar + H has for six h.

S5: As a consecutive to S4, the target was previously exposed to Ar + H for eight h. However, at this stage the gas was switched to argon only, hence after 8 h of exposition to Ar + H, the target was then exposed to argon only during the S5 deposition process.

S6: As a consecutive to S5, the target was exposed to only Ar for the previous two h.

S7: As a consecutive to S5, the target was exposed to only Ar for the previous two h.

2.2. Zinc Oxide Samples Preparation

These samples were all prepared under the exposure of pure zinc oxide target (99.99%) to the Ar + H gas (9 sccm flow rate, working pressure of 2.3×10^{-3} mbar).

During each sample preparation, the chamber was placed under vacuum until it reached a base pressure of 1.5×10^{-7} mbar; three samples (H0, H3, H6) were prepared using 150 W RF plasma power with a working gas pressure of 2.3×10^{-3} for exactly 3 h under the following protocol.

H0: During the preparation of this ZnO deposition, the target had not been previously exposed to Ar+H gas.

H3: As a consecutive to H0 preparation, the target was previously exposed to Ar + H gas for three hours.

H6: As a consecutive to H3, the target was previously exposed to Ar + H gas for six hours.

All the films were consequently characterized using a Zeiss Supra VP35 Field Emission Gun Scanning Electron Microscope equipped with an EDAX Octane Super Energy Dispersive Spectrometer (Ametek, Darmstadt, Germany) (Energy-dispersive X-Ray spectroscopy, EDS) to evaluate the homogeneity and morphology of the film and gather indication on the film chemical composition, in particular the In/Zn ratio (samples S1 to S7) or level of contaminants in the pure ZnO films (samples H0, H3 and H6). The films were also investigated using diffraction techniques, both electron backscatter diffraction (within the Zeiss Supra FEG-SEM equipped with an EDAX DigiView EBSD camera, Darmstadt, Germany) and X-ray diffraction using a Bruker D8 Advance X-Ray Diffractometer with Bragg-Brentano geometry and equipped with a copper tube and LynxEye position-sensitive detector.

Evaluation of the EDS system accuracy and best practice for the chemical analyses of the films was performed using InAs of MAC reference sample #3601. The analyses of the standards were performed at 20 and 10 kV to evaluate the differences in the quantitative analyses (Table 1) and select the optimal conditions. Only atomic percent was under scrutiny because the analyses aimed to identify the ratio of In/Zn in the IZO films following the different deposition conditions.

It can be observed (Table 1) that the system used tends to overestimate the lighter elements both at 20 and 10 kV. When the carbon build-up is considered in the quantification, the atomic % calculation seems to show better agreement with the certified values. The correlation of the quantification at 10 and 20 kV seems to be consistent, however, further overestimation of the lighter elements can be observed at 10 kV.

If this is applied to the films it can be inferred that the measurement at 20 kV is closer to the composition of the films, however, potential underestimation of indium could be applied. In the reference material at 20 kV, a wider scatter of results can be seen, however, the results are constantly closer to the certified results (ratio 1, atomic % 50/50) while the results are more constant at 10 kV, however they are further from the certified values overall.

Theoretically, the results at 10 kV might be more representative of the ratio of In/Zn in the films since the volume of the interaction of the beam is more limited to the surface of the samples, hence, the final spectrum includes only a very limited amount of the elements present in the glass slide which forms the substrate of the film. However, the indication obtained by the presence of carbon build-up in the analysis indicates that an overall evaluation of all elements present in the volume of interaction might be closer to the truthful composition of the material, hence, the data obtained at 20 kV will be used as a characteristic of the films under analyses.

Table 1. Energy-dispersive X-ray spectroscopy (EDS) investigation of the films (S1 to S7) at 10 and 20 kV; the results are presented in atomic % for the calculation of the ratio between the cations. Highlighted in grey are the columns indicating the ratio between the In/Zn cations in the films and In/As cation in the reference material used for the evaluation of the analytical best practice.

Smaple ID	20 kV		Ratio	10 kV		Ratio
	In	Zn		In	Zn	
1	8.04	3.1	2.6	28.7	8.1	3.5
2	14.1	5.2	2.7	40.2	8.4	4.8
3	17.8	5.7	3.1	40	8.4	4.7
4	15	5.3	2.8	37	8	4.6
5	12.4	5.3	2.3	37	9.6	3.9
6	13	5.6	2.3	38	9.5	4
7	14	5.5	2.5	38	8.7	4.4
InAs MAC Reference Material						
Smaple ID	20 kV		Ratio	10 kV		Ratio
	In	As		In	As	
Area 1	47.8	52.2	0.9	46	54	0.9
Area 2	49.4	50.6	1	44	56	0.9
Area 3	47.9	52.1	0.9	46	54	0.9
Area 4	48	52	0.9	46	54	0.9
Area 2 with Carbon built-up	-	-	-	8.1	9.1	0.9
Area 250 μm × 250 μm	-	-	-	46	54	0.9

3. Results

3.1. Flim Morphology, Composition and Crystallinity Characteristics

Secondary electron images of samples S1 to S7 showed a high homogeneity of the film surface (Figure 3A,B). Some samples show oriented linear marks (samples S6 and S7). All samples (using both Ar + H gas and Ar only) show areas with flower-like structures, identifiable as formation islands (Figure 3C,D) with dimensions varying between 1 and 10 microns.

The compositions of the thin films obtained at 20 kV (as discussed above, the validity of the results obtained at different kV was assessed using a reference material to identify which one is most representative, and 20 kV was deemed to be so) show an indium/zinc ratio of 2.3 to 1 to 3.1 to 1, different (higher) from the In_2O_3/ZnO composition obtained by Sheng et al. However, a closer investigation of the results indicates that the presence of the indium ratio in samples deposited with hydrogen is higher than in those deposited with Ar gas alone and sample S5, which represented the switch from Ar + H to Ar gas, shows the lowest In/Zn ratio. Investigation of the crystallinity of the thin films, both using X-ray and electron backscatter diffraction showed that the IZO thin film is amorphous, in agreement with the above-mentioned work of Sheng et al. [12].

Pure ZnO samples (H0, H3 and H6) show an even more distinct granularity (Figure 4A–C) with grains of approximately 100 nm size and heterogenous shape; however, sample H0 shows some defects and a larger less compact grain distribution (Figure 4B) and no "flower-like" structure is visible in any of the ZnO films.

Investigation of the composition of the ZnO films using EDS analyses shows a low concentration of nickel and copper, aside from the zinc and oxygen and from the elements deriving from the substrate glass (Ca, K, Si, Al, Mg).

The nickel is constantly detected at 0.2 wt % in H0 and H3, while iron varies from not detected to 0.2 wt % in these two samples. In H6, nickel is still detected from 0.2 to 0.3 wt %, while iron varies from not detected in the majority of the areas analysed to below 0.2 wt %. Overall, the composition does not show dramatic differences between the three samples, while morphologically, H0 shows larger grains

and a less uniform deposition compared to the other two samples, and the distribution of the grains improves also from H3 to H6, which shows the most uniform aspect (Figure 4A–C).

The ZnO films are fully crystalline, showing the hexagonal ZnO zincite phase (PDF 01-075-1533) with a (1 0 1) preferential orientation.
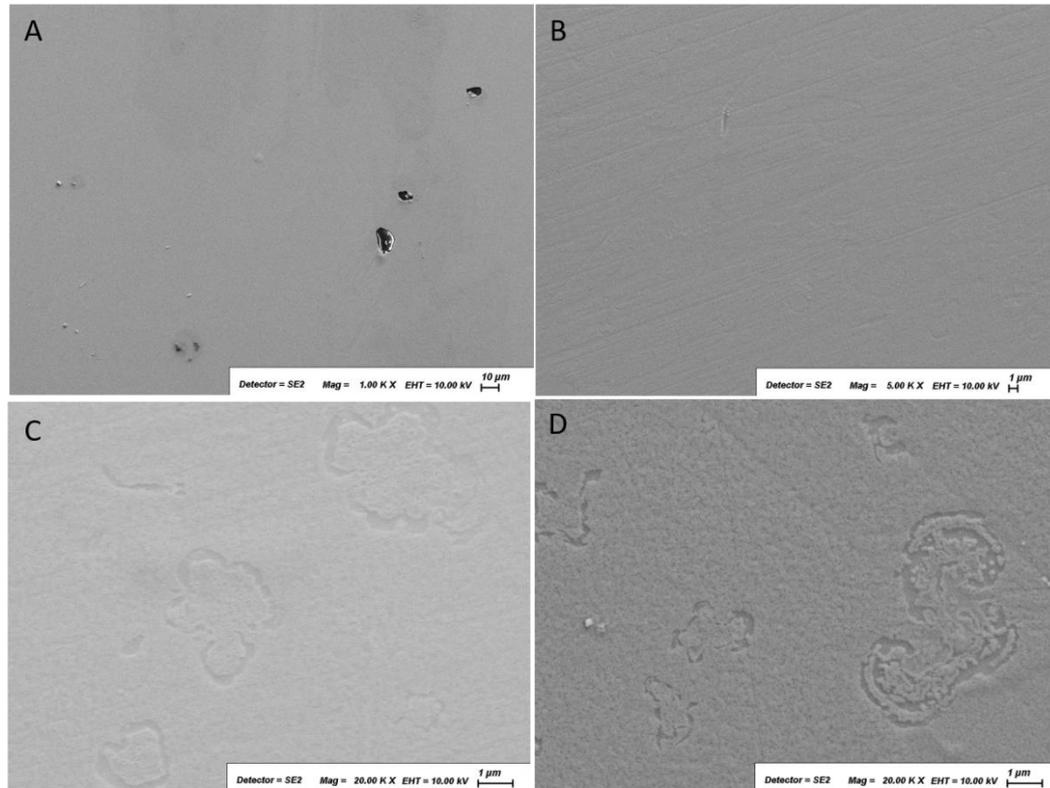

Figure 3. (**A**) The smooth homogenous surface of S6; (**B**) homogenous distribution of the film in sample S7 with an indication of orientation (linear marks); (**C**) secondary electron image of sample S2 showing "flower-like" structures; (**D**) secondary electron image of sample S5 showing "flower-like" structures.
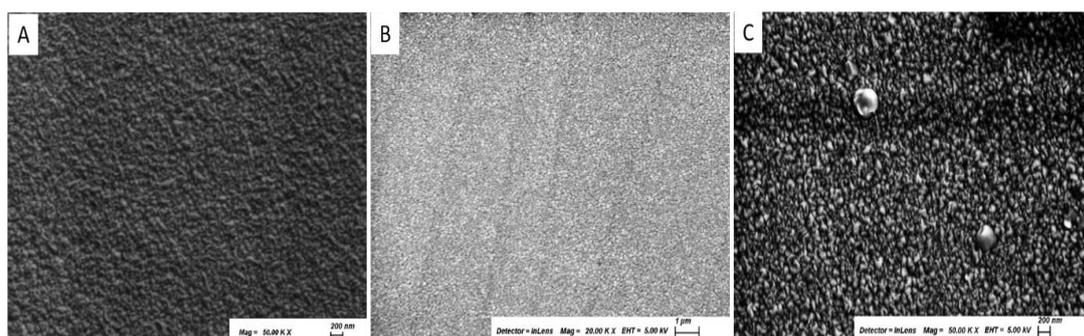
Figure 4. (**A**). In lens image of H6; (**B**) in lens image of H3; (**C**) in lens image of H0 showing larger less homogenous grains and fast carbon build-up during the SEM investigation.

3.2. Electrical Properties

The IZO and ZnO coated substrates were tested for their electrical properties via a four-point probe and Hall effect measurement equipment. The Hall effect samples were 10 mm by 10 mm with contact pads connecting at ~1 mm into the sample from the corners. Figure 5 demonstrates the average sheet resistance of the four substrates belonging to the S1–S7 (IZO) and H0, H3, H6 (ZnO) samples along with the standard deviation of the data. The conductivity of the samples S1–S4 clearly shows

improvement with each consecutive coating under the Ar + H gas. Sample S5 was prepared by switching the gas from Ar + H to Ar gas from the beginning of the process and we observe a very poor electrical conductivity in this sample, while the consistency of the results among the four substrates in the S5 group is significantly poorer than in the other. As for the samples S6 and S7, which were prepared under Ar gas following the processing of S5, there is an improvement in conductivity, but this does not reach the performance of the samples prepared under Ar + H gas (S1–S4).
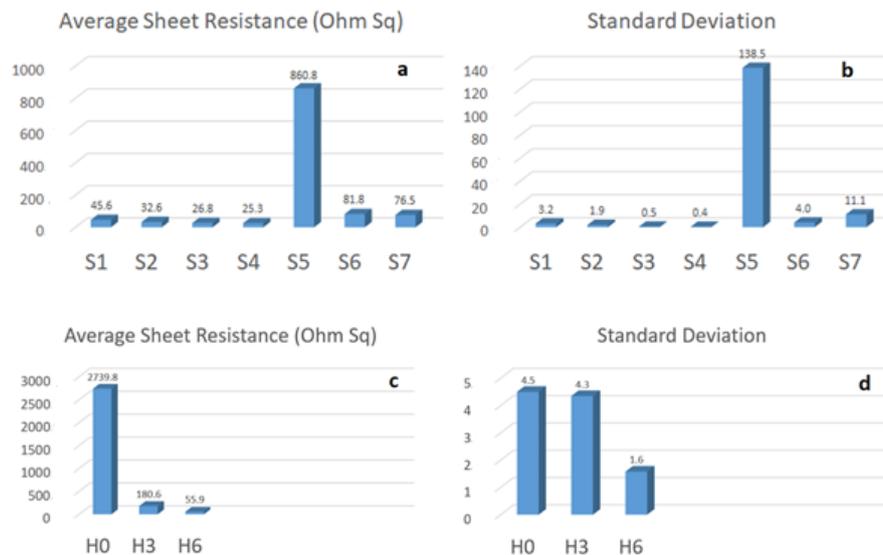
Figure 5. (**a**) The average sheet resistance of the S1–S7 set of samples is presented (four samples from each set). It can be seen that each consecutive deposition process under Ar + H gas gradually improves the sheet resistance of the deposited thin films from S1 to S4. Sample S5 is the sample that was deposited by reverting to Ar gas only. Sample S5 has very poor conductivity. (**b**) From the standard deviation of the obtained sheet resistance data, we can see that during the transition period (S5) even the samples from the same batch demonstrate poor continuity of the property. (**c**) The sheet resistance of the three ZnO samples demonstrates the improvement in sheet resistance of the films due to prolonged exposure to Ar + H gas. (**d**) The standard deviation of the results associated with the ZnO samples.

The ZnO only samples (H0, H3, H6) also clearly demonstrate the effect of consecutive exposure of the target material to the Ar + H gas. These samples, as discussed, were all prepared with Ar + H gas. Sample H0 was prepared with a fresh target, while H3 and H6 were prepared when the target was exposed to 3 and 6 h of Ar + H exposure, respectively. We can see that the electrical conductivity of the samples prepared improves concerning the prior exposure of the gas to Ar + H gas. The H6 sample, which was prepared with longer period of prior exposure to Ar + H gas, was superior to H0 and H3 in terms of electrical properties.

The resistivity of the samples and the thickness of the films are demonstrated in Figure 6. Apart from the sample S1, the rest of the films demonstrate a similar trend in terms of film thickness; however, the resistivity of the samples highlights what we already observed and discussed in Figure 5.

In Figure 7, we can see that the S1–S4 samples have similar mobility values, while the S5 is the poorest, and S6 and S7 are close to the samples coated under Ar + H gas. However, the carrier concentration data suggest that consecutive coating under Ar + H gas further improves the carrier concentration. The carrier concentration in the S4 sample is 5 times higher than the S6 and S7 samples; the S5 transition sample demonstrates the poorest results. The standard deviation values of the average sheet resistance give an indication of the error associated with electrical properties, considering the error associated with mobility and carrier concentration; the 'S' series samples show standard deviation values in the range of (0.33–0.48) for mobility values, with the exception of S5 sample having a standard deviation of 2.8 from the four samples prepared for each series. The standard deviation of carrier

concentration in these samples was in the range of 3.9×10^{18} for S1–S5 and $\sim 3.2 \times 10^{17}$ for S6 and S7. The H series samples show standard deviation values of (0.25–0.33) for mobility and $(3.1–3.9 \times 10^{18})$ for the carrier concentration error in these samples.
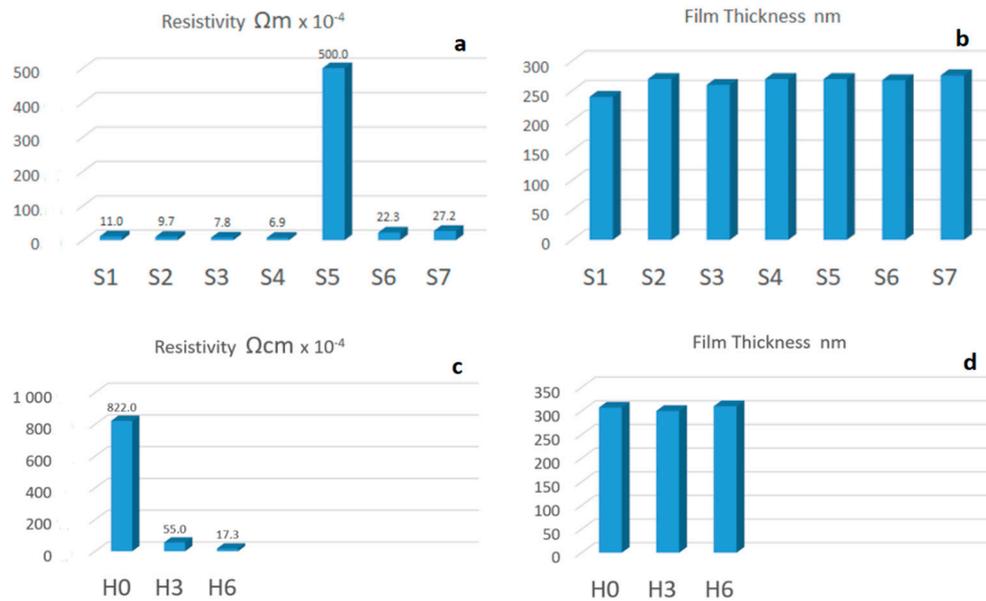

Figure 6. (**a**) The resistivity of the films obtained using the Hall-effect measurement technique demonstrates that each consecutive deposition process under Ar + H gas gradually improves the electrical conductivity of the films, while the S5 sample, deposited during the transition from Ar + H to Ar gas, shows poor results. (**b**) The thickness of the films does not show a significant difference, however, the first sample deposition, where the target was first exposed to hydrogen, demonstrates a lower yield. (**c**) Prolonged exposure to Ar + H gas in improving the resistivity of ZnO based samples. (**d**) All ZnO samples demonstrate similar film thickness.
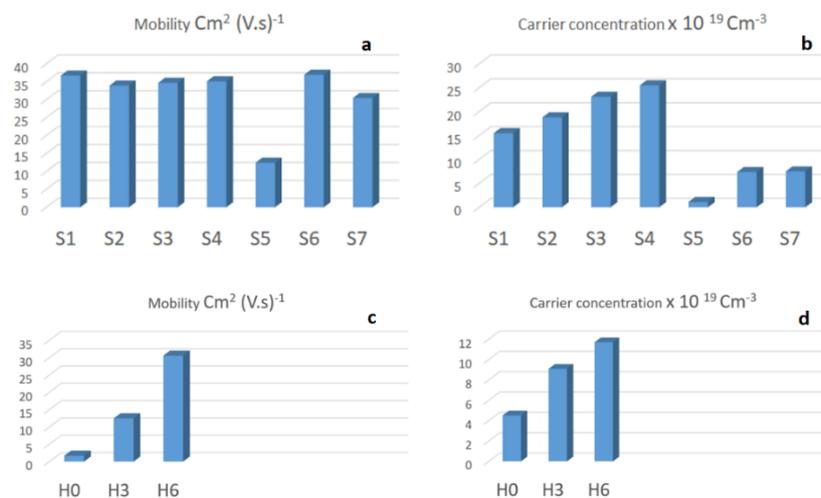

Figure 7. (**a**) Apart from the sample S5, the mobility of the charge carriers does not seem to be affected significantly. (**b**) The carrier concentration seems to be improving with each consecutive deposition under Ar + H gas. The value drops significantly during the transition period where the S5 sample was deposited. The samples S6 and S7, which were coated under Ar gas, show a significantly lower value of carrier concentration compared to the samples coated under Ar + H gas. (**c,d**) In ZnO samples prolonged exposure to the Ar + H gas significantly enhances the mobility and carrier concentration values.

Charge carrier mobility and the carrier concentration are important in determining the electrical conductivity of a material. The mobility of the carriers is a function of carrier recombination time within the material, while the carrier concentration is related to the carrier density. The carrier density in turn is a product of density of states and probability of occupancy.

Both IZO and ZnO samples demonstrate electrical conductivity improvement with consecutive exposure of the target material to Ar + H gas. However, it can be seen that in the case of the IZO sample, the improvement can be traced to enhancement of the carrier concentration values as the mobility values are not significantly affected. This indicates that Ar + H gas processing does not impact the carrier recombination time significantly; however, the increase in carrier concentration indicates the density of states at band level or probability of occupancy of these levels is altered.

In contrast, ZnO samples demonstrate an increase in both mobility and carrier concentration values. It is important to mention that there is a trade-off between increasing carrier concentration and carrier mobility; as carrier concentration increases the probability of charge carrier scattering increases, and as such, overall conductivity would be affected, hence, as is indicated from our results, there is potentially room for further improvement on the ZnO sample until this trade-off is observed. This observation can be further explored to determine the maximum achievable conductivity.

When electrons are traveling through a periodic solid, their movement will be affected by the local forces within the crystal. Thus, a term is used to define the mass of the electrons under that environment, which is referred to as the effective mass. The effective mass, in turn, will be influencing the mobility of the electron (charge carrier). The orbital overlap between the metal cation and the oxygen in the host lattice (e.g., ZnO) is reported to be an important factor in determining the electron mass because metal oxides with predominant s-character of the cation at the CBM are correlated with lowest effective electron masses [13]. The results indicate that the presence of hydrogen in the sputtering gas enhances the mobility of the electrons. This is possibly achieved by hydrogen influencing the oxygen content of the lattice and enhancing the s-characteristic of the indium and zinc. The hydrogen radicals generated in plasma are a strong reducing species [14], and they can withdraw oxygen from the crystal during the deposition. Oxygen vacancy has been believed to play the role of doubly charged donor in In_2O_3 [15,16].

On the other hand, hydrogen atoms can be incorporated in the solid film when they occupy the interstitial site of the crystal. The residing hydrogen forms a hydroxyl bond which may play the role of scattering centre for charge carriers [17]. A separate study on ITO (Indium Tin Oxide) has demonstrated that due to the withdrawal of oxygen during the deposition of ITO films, the hydrogen in plasma can be so effective for achieving lower resistivity that the films were prepared without any sintering [18]. As discussed, our samples were prepared without additional sintering, and achieving highly conductive films without the thermal energy requirement of sintering offers significant commercial benefits.

The hydrogen impurity can be either interstitial or substitutional. Theoretical studies reported by Van de Walle have demonstrated that hydrogen present in ZnO lattice can exclusively behave as an electron donor [19], and this theoretical study is verified by electron nuclear double resonance and Muon spin spectroscopy [20,21].

Considering interstitial locations, computing for formation energies associated with interstitial hydrogen in ZnO indicates that hydrogen is in H^+ state and the H^0 and H^- are not feasible in the ZnO system [21]. The H^+ in the ZnO system will occupy locations within the lattice where it can bind to an oxygen atom and form an O–H bond. This in turn will lead to lattice relaxations resulting in zinc and oxygen experiencing a slight move from their location. Regarding substitutional hydrogen, it is located in the proximity of a nominal oxygen position within the lattice and behaves as a shallow donor [22]. The donor behaviour of the hydrogen impurity in ZnO clearly explains the conductivity observed in ZnO systems and improvement of IZO conductivity.

The electrical conductivity improvements in IZO and ZnO thin films we have observed with the introduction of the hydrogen into the sputtering process are highly important considering the

cost of indium metal and its economic impact at industrial scale TCO production. This means that at industrial scale levels, by applying hydrogen in the process, thinner films of IZO can be produced while the desired electrical conductivity is maintained, and in the case of ZnO, further improvements would eliminate the cost of indium.

For a TCO material to be suitable for most electrode applications, the electrical resistivity (ρ) should be low (10^{-4} to 10^{-5} ohm·cm), the charge carrier mobility (μ) maximized to ~60 cm^2 V^{-1} s^{-1} and the carrier concentrations be kept at about 2×10^{21} cm^{-3} to minimize optical absorption [23]. The charge mobility presented in our results does not match these expectations yet, however, the improvement with using hydrogen could be exploited further by altering the amount of hydrogen, plasma power and chamber pressure, which will be pursued in future work.

The addition of the hydrogen during the sputtering procedure has been reported to cause a drop in the ionization discharge and Ar ion densities [24–27]. Some have also reported yield reduction with introducing hydrogen [28,29] due to the low mass of hydrogen, but we did not observe this in our results; this can be explained by the formation of ArH + ions. Within the plasma, ArH + ions are formed which possess high kinetic energy during target bombardment compared to Ar ions [29]. The film thickness analysis shows that the presence of hydrogen in the plasma has not affected the yield, and the bombardment of the target surface by the ArH + heavy ions could be an explanation for this.

3.3. UV-Vis Spectroscopy

The optical transparency of the films was examined using UV-Vis spectroscopy, and the results are presented in Figure 8. As the four samples within each deposition procedure (S1, S2, H6) demonstrated a similar result, only 'one' sample from each set was used for these measurements (the results do not represent average values). Samples coated under Ar + H demonstrate very similar results with a clear indication of a wider bandgap allowing more light in the 320–430 nm region, and the samples coated under Ar are also very similar within their group. The S5 sample, which so far has been demonstrating poor performance in electrical properties, is no different than the S6 and S7 samples, which were also coated under Ar gas. The ZnO based samples (H series) demonstrate a wider transmission spectrum covering the shorter wavelengths, however, their band gap value is smaller than the IZO samples.

Through the absorption data obtained, by applying a Tauc plot, the optical bandgap of the films was calculated, and the data are presented in Figure 9. The samples S1–S4, which were prepared under Ar + H, demonstrate a wider optical band gap, while the samples S5–S7 demonstrated a smaller optical bandgap. Here, the S5 sample again demonstrates smaller optical wavelength. The H series samples (ZnO) demonstrate an increase in optical band gap values as a result of prolonged exposure of the target to ArH gas.

3.4. Spectral and Colour Function Analysis of the Plasma

The emission characteristics in terms of the whole spectral plot and the chromaticity index were obtained for each test group over two hours. Figure 10 represents the x and y coordinate values of the plasma colour during the transition from Ar gas to Ar + H and vice versa. As we previously had reported, the shifting of the *x* and *y* coordinates during Ar to Ar + H gas are swift compared to the data obtained when switching from Ar + H to Ar, as was the case during the preparation of the S5 sample. We can see that it takes more than one hour for the x and y coordinates to reach their initial value. This indicates that the plasma during this transition period is not stable and is changing. The colour function approach, although still immature, bears the potential of becoming an ideal industrial-scale real-time monitoring system of the process control due to its simplicity of understanding for the operators. Although the colour function method of monitoring the plasma as a diagnostic tool is demonstrating useful applications, from our results we observe significant variations in the 300–400 nm of the spectrum obtained from the plasma, which is not accounted for in the constructing of the x and y chromaticity coordinates.
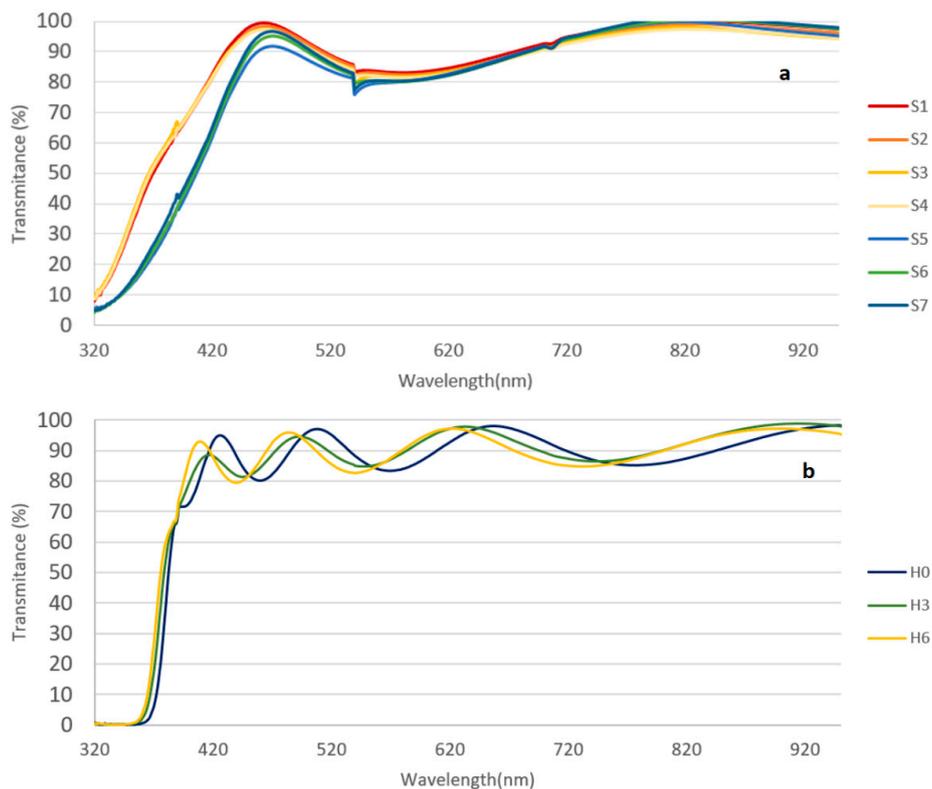
Figure 8. The UV-Vis spectral analysis of the samples in % transmittance is presented. (**a**) IZO samples; from 320 to 470 nm, the samples coated under Ar + H gas demonstrate a wider transmittance range compared to the ones coated under Ar only. From 470 to 1000 nm, all samples demonstrate similar transmittance values. (**b**) ZnO samples; these demonstrate similar transmittance however showing a wider transmission window compared to the IZO based samples.

This indicates that the introduction of hydrogen not only affects the plasma and the specifics of the deposited IZO and ZnO thin film, rather we can conclude that hydrogen is altering the target material itself and possibly forms surface compositions on the target that tend to affect the coating procedure. This can only be confirmed by surface analysis of the target post deposition, which will be investigated by the authors in the future.

Given the specific characteristics of the S5 sample and the shifting of the colour functions during the transition from Ar + H to Ar, we focused on presenting and examining the plasma emissions during the S5 deposition process. The spectral data of the S5 sample at every 100 nm interval from 300 to 900 nm at various stages (from 1 s after the deposition process to 100, 1000, 3000 and 6000 s) of the process of the samples were examined. For simplicity, the 300 to 400 nm segment of the emission spectra is presented in Figure 11 as an example, and the rest of the spectral segments are discussed. From the spectral data it is observed that some emission peaks demonstrate an increase, decrease or no change through the deposition process.

We can identify and refer to some of these peaks using the NIST database (National Institute of Standards and Technology, Gaithersburg, MD, USA). Figure 11 represents the 300–400 nm segment of the emission spectra of the plasma. Here, for example, we can see that the emission at 303.94 nm belonging to oxygen (II) in association with the transition 2s22p2(3P)3d 4D 5/2 to 2s22p2(3P)5f D 2[3]° 7/2 is gradually increasing along with the emission at 326.09 nm belonging to oxygen (III) in association with the transition 2s22p(2P°)3p 3D 2 to 2s22p(2P°)3d 3F° 3. In Figure 11, we also observe a decrease in the 357.07 nm emission peak belonging to argon (II) in association with the transition 3s23p4 (1D) 4p 2D° 3/2 to 3s23p4(3P) 5d 4P 3/2. There is also an increase in the 360.58 nm belonging to argon (II) in association with the 3s23p4(3P)3d 2P 3/2 to 3s23p4(1D)4p 2D° 5/2 transition.
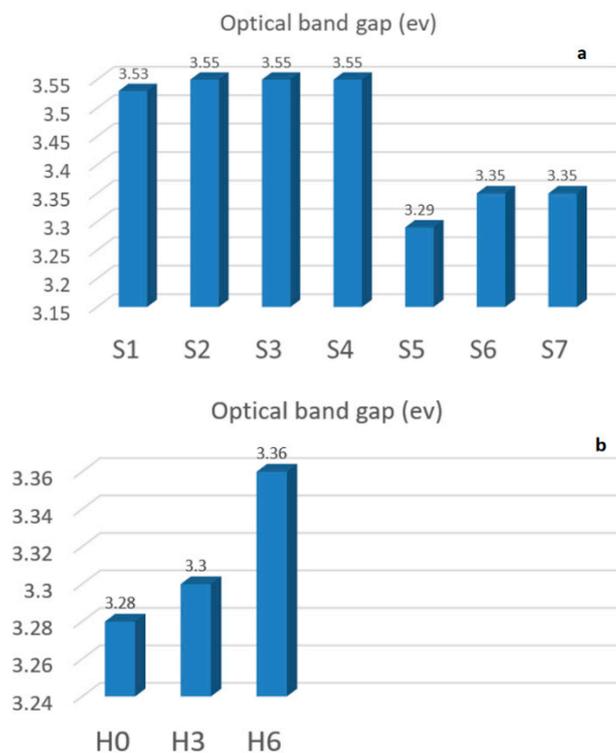
Figure 9. (**a**) The optical band gap of the deposited IZO films was calculated via a Tauc plot. The samples deposited by Ar+H gas demonstrate a wider optical band gap, while the samples coated under Ar gas have a slightly narrower bandgap. The transition sample S5, has the narrowest bandgap. (**b**) In ZnO samples, prolonged exposure to the ArH gas seems to slightly increase the optical bandgap of the material.
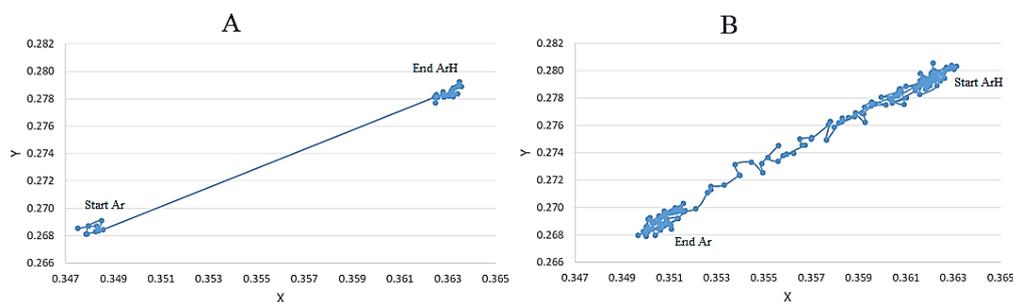

Figure 10. (**A**) The chromaticity colour functions, x and y, are plotted during the transition from Ar to ArH as the deposition of the S1 samples is undertaken. An instant jump in the index values is observed. (**B**) The switch to the Ar gas from the ArH during the S5 sample deposition demonstrates a gradual chaotic variation of the index values is observed, which is in an indication of unstable plasma emissions.

In the 400–500 nm segment of the emission spectra of the plasma, we can see an increase at 410.2 nm which is typically associated with an oxygen (II) transition with the 2s22p2(3P)3p 4P° 1/2 to 2s22p2(3P)3d 4D 1/2 transition. There is also another peak at 451.07 nm, which is associated with Ar (I) 3s23p5(2P°1/2)4s 2[1/2]° 1 to 3s23p5(2P°3/2)5p 2[1/2] 0 transition, which also demonstrates a gradual increase.

In the 500–600 nm range, we observe a decrease at 560.6 nm belonging to argon (I) in association with the 3s23p5(2P°3/2)4p 2[1/2] 1 to 3s23p5(2P°3/2)5d 2[1/2]° 1 transition. There are many other peaks which can also be seen increasing during the preparation of the S5 sample in this region.

In the 600–900 nm range, results indicate that variations in peak intensity or the area covered under the spectrum are not significantly affected.
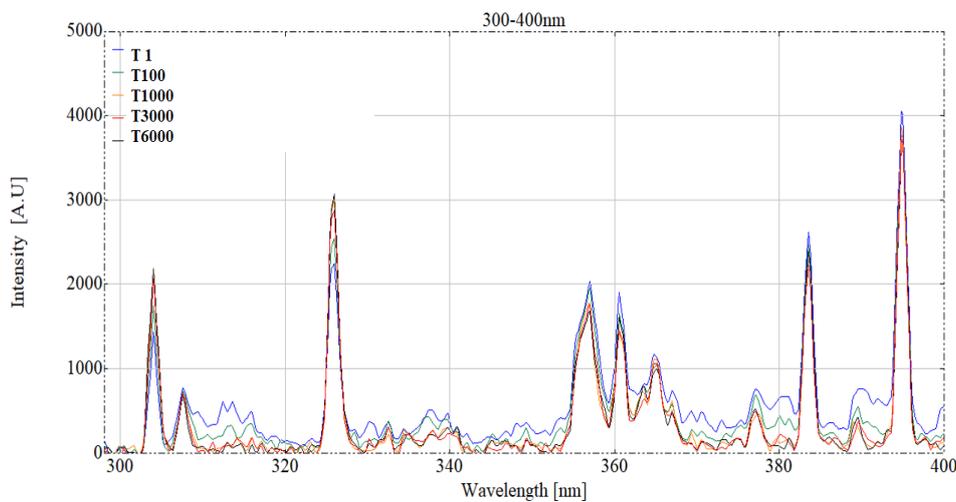
Figure 11. The detailed emission spectra of the plasma between 300 and 400 nm during the deposition of the S5 sample are presented. Three of the peaks demonstrate a gradual intensity increase at time intervals of 1, 100, 1000, 3000 and 6000 s post plasma ignition, while the rest of the spectrum demonstrates a gradual decrease. This region of the spectrum demonstrates significant changes, yet it has not been utilized in colour function calculations.

There have been some reports on the emission line intensity variations when hydrogen is introduced into an argon discharge along with ionization variations with hydrogen introduction [30,31]. However, all these studies require time-consuming efforts and data analysis at micro levels in terms of interpreting the data, which may not be easy to apply during the deposition process.

As hydrogen is added to the Ar magnetron discharge, the plasma parameters in the discharge begin to change. Studies on plasma behaviour during the preparation of TiO_2 films have shown that the addition of hydrogen to oxygen-containing argon discharge leads to a continuous decrease of electron density and a corresponding increase of electron temperature from 6.30 to 6.74 eV [32]. The increase in electron temperature can be accounted for by the reduction of the value of electron density in the discharge.

For a good approximation in low-pressure discharge, the emission intensity of a particular line of an element is considered to be proportional to the density of that particular species [33,34]. Comparing the line intensity ratio of selected transitions, one can estimate the degree of dissociation and ionization of particular species present in the discharge. The line intensity ratios of IH/IAr can be used to determine the degree of dissociation in hydrogen plasma using the following relation [35]:

$$N_H = k\frac{I_H}{I_{Ar}}$$

where N_H and N_{Ar} are the degrees of dissociation of hydrogen and argon, and *k* is a parameter related to the rate coefficients for direct excitation of the corresponding Ar and H atoms and the radiation transition probabilities and lifetimes of the corresponding excited states respectively.

As discussed earlier we can see an increase in the intensities associated with certain argon and oxygen transitions during the Ar + H gas switch to Ar only. The detailed study of the plasma is beyond the scope of this research; however, from these results, we can see that once the target material is exposed to the Ar + H gas, the process of reverting the plasma condition to a prior state is time dependent. The sample S5, which was prepared during such a process, is the result of a continuously changing plasma condition, and as such, we see the properties of the film are directly affected. The colour function approach, as demonstrated in Figure 10, also verifies this. Hence, the colour function approach can be considered a simpler approach toward monitoring the status of the plasma when significant details are not required.

4. Conclusions

We have demonstrated that the deposition of IZO and ZnO film under a reducing atmosphere can enhance the electrical property of these thin films by enhancing the carrier concentration of IZO films and increasing the carrier concentration and mobility in ZnO films. Most importantly, we present clear evidence that consecutive exposure of the target material to Ar+H gas will to some extent add further improvements to the electrical properties. A target that has been previously exposed to Ar+H gas seems to be altered at the surface, as reverting to Ar gas only for deposition will initially produce a thin film with inconsistent electrical properties.

The improvements obtained with introducing hydrogen during the sputter deposition of IZO can minimise the consumption of indium, as thinner films with identical electrical properties can be deposited. In the case of further improvements with the electrical properties of pure ZnO thin films, introduction of hydrogen can potentially lead to the elimination of indium. As such, there can be significant commercial benefits in depositing the ZnO based family of TCOs under Ar+H gas mix, if the need for indium and high-temperature sintering is avoided; however, further improvement and assessment are required.

We have demonstrated that by applying colour function analysis we can visualize the status of the plasma stability. During the sputter deposition of IZO under argon, when the target has been previously exposed to hydrogen, we see an unstable plasma and an IZO film with very poor performance, resulting also in the lowest concentration of indium. The fact that the chromaticity index values (x and y) do not swiftly fall back to the values expected for argon indicates that for the surface modifications caused by hydrogen to revert to the original state, a layer from the target has to be removed, leading to a film with poor charge carrier and density properties. The colour function evaluation of the plasma can be a beneficial observational tool for monitoring the plasma during system operations. However, further work is required to mature this method of plasma monitoring and assessment. Hence, our next task will be to investigate the plasma emissions and, if necessary, formulate a new colour function that takes into account the emissions in the 300–400 nm region. This will lead to constructing a new colour coordinate system that will specifically define the colour of plasma, similar to how the colours in the visible spectrum are defined by the x and y index values.

Author Contributions: Conceptualization, A.S.; Methodology, A.S.; Software, A.H.; Validation, H.U., L.A. and A.S.; Formal analysis, U.O.; Investigation, A.S.; Resources, H.U.; Data curation, A.A.; Writing—original draft preparation, A.S.; Writing—review and editing, A.S.; Visualization, C.S.; Supervision, H.U.; Project administration, H.U.; Funding acquisition, H.U. All authors have read and agreed to the published version of the manuscript.

Conflicts of Interest: The authors declare no conflict of interest.

References

1. Morales-Masis, M.; Nicolas, S.M.D.; Holovsky, J.; Wolf, S.D.; Ballif, C. Low temperature high-mobility amorphous IZO for silicon heterojunction solar cells. *IEEE J. Photovolt.* **2015**, *5*, 1340–1347. [CrossRef]
2. Hagendorfer, H.; Lienau, K.; Nishiwaki, S.; Fella, C.M.; Kranz, L.; Uhl, A.R.; Jaeger, D.; Luo, L.; Gretener, C.; Buecheler, S.; et al. Highly transparent and conductive ZnO: Al thin films from a low-temperature aqueous solution approach. *Adv. Mater.* **2014**, *26*, 632–636. [CrossRef]
3. Burschka, J.; Pellet, N.; Moon, S.J.; Humphry-Baker, R.; Gao, P.; Nazeeruddin, M.K.; Grätzel, M. Sequential deposition as a route to high performance. *Nature* **2013**, *499*, 316–319. [CrossRef] [PubMed]
4. Martins, R.; Almeida, P.; Barquinha, P.; Pereira, L.; Pimentel, A.; Ferreira, I.; Fortunato, E. Electron transport and optical characterization amorphous indium zinc oxide films. *J. Non-Cryst. Solids* **2006**, *352*, 1471–1474. [CrossRef]

5.　Taylor, M.P.; Readey, D.W.; van-Hest, M.F.A.M.; Teplin, C.W.; Alleman, J.L.; Dabney, M.S.; Gedvillas, L.M.; Keyes, B.M.; To, B.; Perkins, J.D.; et al. The remarkable thermal stability of amorphous In-Zn-O transparent conductors. *Adv. Funct. Mater.* **2008**, *18*, 3169–3178. [CrossRef]

6.　Koida, T.; Michio, K.; Koichi, T.; Akio, S.; Michio, S.; Hiroyuki, F. Hydrogen-doped In2O3 transparent conducting oxide films prepared by solid-phase crystallization method. *J. Appl. Phys.* **2010**, *107*, 033514. [CrossRef]

7.　Park, Y.R.; Nam, E.; Boo, J.; Jung, D.; Suh, S.J.; Kim, Y.S. Hydrogenated In-doped ZnO thin films for the new anode material of organic light-emitting devices: Synthesis and application test. *Bull. Korean Chem. Soc.* **2007**, *28*, 2396–2400.

8.　Park, Y.R.; Kim, J.; Kim, Y.S. Growth and characteristics of hydrogenated In-doped ZnO thin films by pulsed DC magnetron sputtering. *Appl. Surf. Sci.* **2009**, *256*, 1589–1594. [CrossRef]

9.　Kahn, A. Fermi level, work function, and vacuum level. *Mater. Horiz.* **2016**, *3*, 7–10. [CrossRef]

10.　Burstein, E. Anomalous optical absorption limit in InSb. *Phys. Rev.* **1954**, *93*, 632–633. [CrossRef]

11.　Salimian, A.; Haghpanahan, R.; Hasnath, A.; Upadhyaya, H. Optical analysis of RF sputtering plasma through color characterization. *Coatings* **2019**, *9*, 315. [CrossRef]

12.　Sheng, J.; Lee, H.-J.; Oh, S.; Park, J.S. Flexible and high-performance amorphous indium Zinc oxide thin-film transistor using low-temperature atomic layer deposition. *ACS Appl. Mater. Interfaces* **2016**, *8*, 33821–33828. [CrossRef] [PubMed]

13.　Hautier, G.; Miglio, A.; Waroquiers, D.; Rignanese, G.-M.; Gonze, X. How does chemistry influence electron effective mass in oxides? A high-throughput computational analysis. *Chem. Mater.* **2014**, *26*, 5447–5458. [CrossRef]

14.　Wallinga, J.; Arnold Bik, W.M.; Vredenberg, A.M.; Schropp, R.E.I.; van der Weg, W.F. Reduction of Tin Oxide by Hydrogen Radicals. *J. Phys. Chem. B* **1998**, *102*, 6219. [CrossRef]

15.　De Wit, J.H.W. Electrical properties of In2O3. *J. Solid State Chem.* **1973**, *8*, 142. [CrossRef]

16.　Dewit, J.H.W.; Vanunen, G.; Lahey, M. Electron concentration and mobility in In2O3. *J. Phys. Chem. Solids* **1997**, *38*, 819–824. [CrossRef]

17.　Luo, S.; Kohiki, S.; Okada, K.; Kohno, A.; Tajiri, T.; Arai, M.; Shoji, F. Effects of Hydrogen in Working Gas on Valence States of Oxygen in Sputter-Deposited Indium Tin Oxide Thin Films. *Acs Appl. Mater. Interfaces* **2010**, *2*, 663–668. [CrossRef]

18.　Dixon, S.C.; Scanlon, D.O.; Carmalt, C.J.; Parkin, I.P. *n*-Typed doped transparent conductive binary oxides: An overview. *J. Mater. Chem. C* **2016**, *4*, 6946–6961. [CrossRef]

19.　Van de Walle, C.G. Hydrogen as a Cause of Doping in Zinc Oxide. *Phys. Rev. Lett.* **2000**, *85*, 1012–1015. [CrossRef]

20.　Hofmann, D.M.; Hofstaetter, A.; Leiter, F.; Zhou, H.; Henecker, F.; Meyer, B.K.; Baranov, P.G. Hydrogen: A Relevant Shallow Donor in Zinc Oxide. *Phys. Rev. Lett.* **2002**, *88*, 045504. [CrossRef]

21.　Cox, S.F.J.; Davis, E.A.; Cottrell, S.P.; King, P.J.C.; Lord, J.S.; Gil, J.M.; Alberto, H.V.; Vilo, R.C.; Piroto Duarte, J.; Ayres de Campos, N.; et al. Experimental Confirmation of the Predicted Shallow Donor Hydrogen State in Zinc Oxide. *Phys. Rev. Lett.* **2001**, *86*, 2601–2604. [CrossRef] [PubMed]

22.　Van de Walle, C.G. Hydrogen as a shallow center in semiconductors and oxides. *Phys. Status Solidi* **2003**, *235*, 89–95. [CrossRef]

23.　Knewstubb, P.F.; Tickner, A.W. Mass spectrometry of ions in glow discharges. I. apparatus and its application to the positive column in rare gases. *J. Chem. Phys.* **1962**, *36*, 674. [CrossRef]

24.　Gordon, M.H.; Kruger, C.H. Non-equilibrium effects of diluent addition in a recombining argon plasma. *Phys. Fluids B Plasma Phys.* **1993**, *5*, 1014. [CrossRef]

25.　Meulenbroeks, R.F.G.; van Beek, A.J.; van Helvoort, A.J.G.; van de Sanden, M.C.M.; Schram, D.C. Argon-hydrogen plasma jet investigated by active and passive spectroscopic means. *Phys. Rev. E* **1994**, *49*, 4397–4406. [CrossRef] [PubMed]

26.　Mason, R.S.; Miller, P.D.; Mortimer, I.P. Anomalous loss of ionization in argon-hydrogen plasma studied by fast flow glow discharge mass spectrometry. *Phys. Rev. E* **1997**, *55*, 7462–7472. [CrossRef]

27.　Tabares, F.L.; Tafalla, D. Sputtering of metallic walls in Ar/H$_2$ direct current glow discharges at room temperature. *J. Vac. Sci. Technol. A* **1996**, *14*, 3087–3091. [CrossRef]

28.　Budtz-Jorgensen, C.V.; Kringhoj, P.; Bottiger, J. The critical role of hydrogen for physical sputtering with Ar–H$_2$ glow discharges. *Surf. Coat. Technol.* **1999**, *116*, 938–943. [CrossRef]

29. Smithwick, R.W., III; Lynch, D.W.; Franklin, J.C. Relative ion yields measured with a high-resolution glow discharge mass spectrometer operated with an argon/hydrogen mixture. *J. Am. Soc. Mass Spectrom.* **1993**, *4*, 278–285. [CrossRef]

30. Saito, M. The relationship between relative sensitivity factors and ionization potential in dc glow discharge mass spectrometry using Ar/0.2 vol.% H_2 mixture. *Anal. Chim. Acta.* **1997**, *355*, 129–134. [CrossRef]

31. Saikia, P.; Saikia, B.K.; Bhuyan, H. Study on the effect of hydrogen addition on the variation of plasma parameters of argon-oxygen magnetron glow discharge for synthesis of TiO2 films. *Aip Adv.* **2016**, *6*, 045206. [CrossRef]

32. Kakati, H.; Pal, A.R.; Bailung, H.; Chutiya, J. Effect of oxygen on the characteristics of radio frequency planar magnetron sputtering plasma used for aluminum oxide deposition. *J. Appl. Phys.* **2007**, *101*, 083304. [CrossRef]

33. Coburn, J.W.; Chen, M. Optical emission spectroscopy of reactive plasmas: A method for correlating emission intensities to reactive particle density. *J. Appl. Phys.* **1980**, *51*, 3134–3136. [CrossRef]

34. Lavrov, B.P.; Pipa, A.V.; Röpcke, J. On determination of the degree of dissociation of hydrogen in non-equilibrium plasmas by means of emission spectroscopy: I. The collision-radiative model and numerical experiments. *Plasma Sources Sci. Technol.* **2006**, *15*, 135–146. [CrossRef]

35. Clay, K.J.; Speakman, S.P.; Amaratunga, G.A.J.; Silva, S.R.P. Characterization of a-C: H: N deposition from CH4/N2 rf plasmas using optical emission spectroscopy. *J. Appl. Phys.* **1996**, *79*, 7227–7233. [CrossRef]